

Accuracy and Stability of the Coarse Time-Stepper for a Lattice Boltzmann Model

Christophe Vandekerckhove

Pieter Van Leemput

Dirk Roose

Report TW 501, September 2007



Katholieke Universiteit Leuven
Department of Computer Science
Celestijnenlaan 200A – B-3001 Heverlee (Belgium)

Accuracy and Stability of the Coarse Time-Stepper for a Lattice Boltzmann Model

Christophe Vandekerckhove

Pieter Van Leemput

Dirk Roose

Report TW 501, September 2007

Department of Computer Science, K.U.Leuven

Abstract

The equation-free framework for multiscale computing is built around the central idea of a coarse time-stepper, which is an approximate time integrator for the unavailable macroscopic model when only a microscopic simulator is given. In this paper, we study the numerical properties of the coarse time-stepper when a lattice Boltzmann model for one-dimensional diffusion is used as the microscopic simulator. We derive analytical expressions for the accuracy and stability of the coarse time-stepper, which allow us to study the influence of various aspects involved its construction.

Keywords : equation-free multiscale computing, lattice Boltzmann model, accuracy, stability

Accuracy and Stability of the Coarse Time-Stepper for a Lattice Boltzmann Model

Christophe Vandekerckhove, Pieter Van Leemput and Dirk Roose

Department of Computer Science, Katholieke Universiteit Leuven,
B-3001 Heverlee, Belgium

Abstract

The equation-free framework for multiscale computing is built around the central idea of a coarse time-stepper, which is an approximate time integrator for the unavailable macroscopic model when only a microscopic simulator is given. In this paper, we study the numerical properties of the coarse time-stepper when a lattice Boltzmann model for one-dimensional diffusion is used as the microscopic simulator. We derive analytical expressions for the accuracy and stability of the coarse time-stepper, which allow us to study the influence of various aspects involved its construction.

Keywords: equation-free multiscale computing, lattice Boltzmann model, accuracy, stability

1 Introduction

For an important class of multiscale problems, the available model is given on a microscopic level, while we would like to analyze the system on a much coarser, macroscopic level. The microscopic model may for instance describe the complex interactions between a large number of atoms or molecules, while we are only interested in certain macroscopic quantities such as the particle density field. Conceptually, we could then start a simulation with the microscopic model and extract the evolving particle density field. Due to the large amount of particles and the presence of fast time and short space scales, this is however only computationally feasible over a spatio-temporal domain that is much smaller than the domain over which the macroscopic fields typically evolve.

To bridge this gap between the (microscopic) scale of the available model and the (macroscopic) scale of interest, one traditionally attempts to derive a macroscopic description from the microscopic model. For the example above, this could for instance result in a partial differential equation (PDE) for the evolution of the particle density field.

For some problems, it may however be difficult or undesirable to derive an accurate macroscopic model, although it should exist conceptually. For this class of problems, the equation-free framework was developed [8]. It allows the modeler to perform macroscopic tasks efficiently, even when no macroscopic equation is available (hence the name “equation-free”). The framework is built around the central idea of a coarse time-stepper (CTS), which maps macroscopic variables at time t_n to macroscopic variables at time $t_{n+1} = t_n + \Delta T$, using only the microscopic simulator. The ultimate goal of the CTS is to be an approximate time-stepper for the unknown macroscopic equation. (As in [8], we use “time-stepper” as a synonym for “time integrator”.) One step of the CTS consists of three substeps: (1) *lifting*, in which the macroscopic state at time t_n is transformed to an appropriate higher-dimensional microscopic state, (2) *simulation*, in which the microscopic realization is evolved over time ΔT using the microscopic simulator, and (3) *restriction*, in which the detailed microscopic solution is transformed back to a macroscopic state at time t_{n+1} . In some cases, it may be required to evolve more microscopic realizations simultaneously in the procedure above, e.g. when the microscopic simulator is stochastic or chaotic.

The CTS can subsequently be used as “input” for time-stepper based numerical algorithms performing macroscopic tasks. For example, coarse projective integration [4, 8] or one of the related time integration techniques from [2, 5, 9, 18, 17] can then be used to compute the transient behavior of the macroscopic variables in an efficient way. Other tasks such as bifurcation analysis, optimization or control of the unavailable macroscopic equation have also been explored, see e.g. [13, 14, 8, 10, 12].

In several papers [13, 6, 8, 14, 15], the equation-free approach was studied using a lattice Boltzmann model (LBM) for a reaction-diffusion system as the microscopic simulator. Such a LBM is a simplified kinetic model that incorporates the essential microscopic physics such that the macroscopic averaged properties obey the desired macroscopic equations (therefore a LBM is actually a mesoscopic rather than a microscopic model). Since the corresponding macroscopic equation can be derived for this model problem (it is the classical reaction-diffusion PDE), it provides us, next to the solution of the LBM itself, with a reference solution that can be used in the analysis of the equation-free methods (which should in practice of course only be used when the macroscopic equation is *not* available). Also, while most microscopic models are stochastic in nature, the LBM is a deterministic model as it involves ensemble averages (distribution functions) rather than individual particles. Although the understanding of the influence of statistical noise is vital for the further development of the equation-free framework, the absence of stochastic noise in the LBM allows us to study the numerical properties of the CTS, such as accuracy and stability, in a more traditional way.

In the papers mentioned above, various aspects of the equation-free framework (such as using coarse projective integration or coarse numerical bifurcation analysis) were studied mainly *numerically*. In this paper, we take a step back and focus on the CTS itself when the LBM for a one-dimensional diffusion system is used as the microscopic simulator. Although the results in this paper could easily be extended to systems including reactions, we have chosen not to do this as it does not add essential insight. Due to the simplicity of the LBM, we are able to derive *analytical* expressions for the accuracy and stability of the CTS. These expressions depend on the LBM parameters but also on the implementation of the CTS. Hence, the analysis allows us to compare the influence of various aspects involved in the construction of the CTS in a systematic way. The results obtained in this paper also contribute substantially to the understanding of the numerical results in [13, 6, 8, 14, 15], and they may be useful for the further analysis and/or development of the equation-free methods.

This paper is organized as follows. In Section 2, we present the LBM and show its relation to the macroscopic equation and a corresponding macroscopic time-stepper. In Section 3, we work out several alternative implementations for the substeps in the CTS. The accuracy and stability of the CTS, based on these different implementations, is studied in Section 4. Finally, we summarize our findings and draw conclusions in Section 5.

2 The LBM and the corresponding macroscopic equation

In Section 2.1, we first formulate the LBM that will be used as a model problem throughout this paper. In Section 2.2, we then describe its relation with the macroscopic equation, which can be derived using a Chapman-Enskog multiscale expansion. Finally, in Section 2.3, we briefly summarize the accuracy and stability properties of a typical time-stepper for the macroscopic equation. The latter will guide the analysis of the CTS in Section 4.

2.1 The LBM

A LBM [1] describes the evolution of discrete particle distribution functions $f_i(x_j, t_k)$, which depend on space x_j , time t_k and velocity v_i . For our one-dimensional model problem, only three values are considered for the velocity ($v_i = i\Delta x/\Delta t$, with $i \in \{-1, 0, 1\}$), and each distribution function f_i is discretized in space on the domain $[0, 1]$ using a grid spacing $\Delta x = 1/N$ (N lattice intervals) and in time using a time step Δt . In the interior of the spatial domain, the LBM

evolution law for the distributions $f_i(x_j, t_k)$ is then

$$f_i(x_{j+i}, t_{k+1}) = f_i(x_j + i\Delta x, t_k + \Delta t) = f_i(x_j, t_k) - \omega (f_i(x_j, t_k) - f_i^{eq}(x_j, t_k)), \quad (1)$$

with $i \in \{-1, 0, 1\}$. The parameter ω is called the relaxation coefficient, and, for reasons that will become clear later on, its value is confined to the interval $(0, 2)$. Each time step of the LBM scheme naturally decouples into two phases. First, the distribution functions $f_i(x_j, t_k)$ are updated. Afterwards, they propagate to a neighboring lattice site according to their velocity direction. At the boundaries, we impose Dirichlet boundary conditions $\rho(0, t_k) = \rho(1, t_k) = 0$ (with $\rho(x_j, t_k)$ the particle density field as defined in equation (3) below) by assigning the appropriate value to the distribution functions that stream into the domain at $x_0 = 0$ and $x_N = 1$.

Diffusive collisions are modeled by the Bhatnagar-Gross-Krook (BGK) collision term — the term $-\omega(f_i(x_j, t_k) - f_i^{eq}(x_j, t_k))$ in (1) — as a relaxation to a local diffusive equilibrium [11]

$$f_i^{eq}(x_j, t_k) = \frac{1}{3}\rho(x_j, t_k). \quad (2)$$

The particle density field $\rho(x_j, t_k)$ is defined as the zeroth-order velocity moment $f_i(x_j, t_k)$

$$\rho(x_j, t_k) = \sum_{i=-1}^1 f_i(x_j, t_k) = \sum_{i=-1}^1 f_i^{eq}(x_j, t_k), \quad (3)$$

where the second equality expresses that the BGK diffusive collisions locally conserve density. Similarly, we can also define the momentum ϕ and the energy ξ as (a rescaling of) the first and the second order (or in short: the higher order) moments $f_i(x_j, t_k)$

$$\phi(x_j, t_k) = \sum_{i=-1}^1 i f_i(x_j, t_k), \quad \xi(x_j, t_k) = \frac{1}{2} \sum_{i=-1}^1 i^2 f_i(x_j, t_k). \quad (4)$$

Since there is a one-to-one relation between the particle distribution functions $f_{-1}(x_j, t_k)$, $f_0(x_j, t_k)$, $f_1(x_j, t_k)$ and the velocity moments $\rho(x_j, t_k)$, $\phi(x_j, t_k)$, $\xi(x_j, t_k)$, the LBM state is equally well described by each of these variable sets. In this paper, we will further use the moment description, as this will turn out to be a more natural choice in the context of equation-free computing. The LBM state can then be represented by the $(3N+3)$ -dimensional column vector $[\rho^T \phi^T \xi^T]^T$, with ρ , ϕ and ξ the $(N+1)$ -dimensional column vectors corresponding to the spatially discretized velocity moments. By combining (1), (3) and (4), and due to the linearity of the LBM, the action of one LBM step (from time t_k to $t_{k+1} = t_k + \Delta t$) can be described by the matrix-vector product

$$\begin{bmatrix} \rho \\ \phi \\ \xi \end{bmatrix}_{k+1} = S \cdot \begin{bmatrix} \rho \\ \phi \\ \xi \end{bmatrix}_k = \begin{bmatrix} S_{1,1} & S_{1,2} & S_{1,3} \\ S_{2,1} & S_{2,2} & S_{2,3} \\ S_{3,1} & S_{3,2} & S_{3,3} \end{bmatrix} \cdot \begin{bmatrix} \rho \\ \phi \\ \xi \end{bmatrix}_k. \quad (5)$$

Away from the boundaries of the domain, the submatrices $S_{i,j}$ of the constant Jacobian matrix have a tridiagonal structure. The values of the elements on the subdiagonal, diagonal and superdiagonal are given in Table 1 (a detailed derivation is given in [15]). Here, and also further on, e_i will denote a matrix element that is positioned i places above (or, if $i < 0$, below) the diagonal of the matrix.

2.2 Relation to the corresponding macroscopic equation

Through a Chapman-Enskog multiscale expansion [1], one can derive the effective macroscopic equation from the LBM. Neglecting higher order contributions, we obtain the diffusion equation with macroscopic diffusion coefficient D and Dirichlet boundary conditions

$$\frac{\partial \rho(x, t)}{\partial t} = D \frac{\partial^2 \rho(x, t)}{\partial x^2} = \left(\frac{2 - \omega}{3\omega} \frac{\Delta x^2}{\Delta t} \right) \frac{\partial^2 \rho(x, t)}{\partial x^2}, \quad \rho(0, t) = \rho(1, t) = 0. \quad (6)$$

Table 1: The values of e_{-1} , e_0 and e_1 , the elements on the subdiagonal, diagonal and superdiagonal of the Jacobian matrix of the LBM.

	$S_{1,1}$	$S_{1,2}$	$S_{1,3}$	$S_{2,1}$	$S_{2,2}$	$S_{2,3}$	$S_{3,1}$	$S_{3,2}$	$S_{3,3}$
e_{-1}	$\frac{\omega}{3}$	$\frac{1-\omega}{2}$	$1-\omega$	$\frac{\omega}{3}$	$\frac{1-\omega}{2}$	$1-\omega$	$\frac{\omega}{6}$	$\frac{1-\omega}{4}$	$\frac{1-\omega}{2}$
e_0	$1 - \frac{2\omega}{3}$	0	$2(\omega - 1)$	0	0	0	0	0	0
e_1	$\frac{\omega}{3}$	$\frac{\omega-1}{2}$	$1-\omega$	$\frac{-\omega}{3}$	$\frac{1-\omega}{2}$	$\omega-1$	$\frac{\omega}{6}$	$\frac{\omega-1}{4}$	$\frac{1-\omega}{2}$

The fact that the macroscopic behavior can be described in terms of the density ρ only implies that the higher order moments ϕ and ξ become functionals of (slaved to) the density ρ on a time scale that is very short compared to the macroscopic time scales. This separation of time scales, which underpins the existence of the macroscopic equation, is also exploited in the equation-free framework (see further). For our LBM, these functionals, which are often called slaving relations, can be found as a by-product of the Chapman-Enskog expansion. After dropping the indices j and k , and retaining only terms up to third order, we obtain

$$f_i(x, t) \approx \frac{1}{3}\rho(x, t) - \frac{i}{3\omega} \frac{\partial \rho(x, t)}{\partial x} \Delta x - (3i^2 - 2) \frac{\omega - 2}{18\omega^2} \frac{\partial^2 \rho(x, t)}{\partial x^2} \Delta x^2 + i \frac{\omega^2 - 2\omega + 2}{18\omega^3} \frac{\partial^3 \rho(x, t)}{\partial x^3} \Delta x^3$$

for the distribution functions, or in terms of the velocity moments

$$\phi(x, t) = \sum_{p=0}^{\infty} \phi_p(x, t) \Delta x^p = -\frac{2}{3\omega} \frac{\partial \rho(x, t)}{\partial x} \Delta x + \frac{\omega^2 - 2\omega + 2}{9\omega^3} \frac{\partial^3 \rho(x, t)}{\partial x^3} \Delta x^3 + \mathcal{O}(\Delta x^5), \quad (7)$$

$$\xi(x, t) = \sum_{p=0}^{\infty} \xi_p(x, t) \Delta x^p = \frac{1}{3}\rho(x, t) - \frac{\omega - 2}{18\omega^2} \frac{\partial^2 \rho(x, t)}{\partial x^2} \Delta x^2 + \mathcal{O}(\Delta x^4). \quad (8)$$

These slaving relations define a manifold in phase space, which we will further call the “slow manifold”. The macroscopic model (6) is then a description for the dynamics on this slow manifold. If the LBM is initialized away from the slow manifold, the higher order moments will be attracted quickly towards the manifold (due to the time scale separation), after which they evolve on the manifold on a macroscopic time scale according to (7)–(8). Nevertheless, in this case a substantial and persistent macroscopic error may be introduced, as was shown in [14, 19]. The latter can be avoided by initializing on (or very close to) the slow manifold, as the evolution of the higher order moments will then directly be governed by the density field only. The appropriate initialization of the LBM, close enough to the slow manifold, is hence crucial to recover the correct macroscopic behavior when using the full LBM or the CTS for the LBM. This observation will be confirmed by our analysis further on.

A numerical illustration of the slaving relations (7)–(8) is shown in Figure 1. Here, we have chosen $N = 1000$, $\omega = 1.25$ and $D = 1$ (hence, $\Delta t = 2 \cdot 10^{-7}$) and computed the eigenvalue decomposition of the Jacobian matrix S . The eigenvectors corresponding to the three most dominant eigenvalues $\lambda_k \approx 1 - k^2 \pi^2 \Delta t$ ($k = 1, 2, 3$) are shown in the first row of Figure 1. To simplify the interpretation, we split and rescaled the eigenvectors per velocity moment and mapped them onto the spatial domain $[0, 1]$. For the density ρ , we clearly recognize the eigenvalues and the corresponding sinusoidal eigenmodes that are typical for the pure diffusion problem with homogeneous Dirichlet boundary conditions (see also Section 2.3). The differences between the parts of the eigenvectors corresponding to the higher order moments ϕ or ξ , and the slaving relations (7) or (8) up to first or third order terms in Δx are shown in the second and third row of Figure 1. Here,

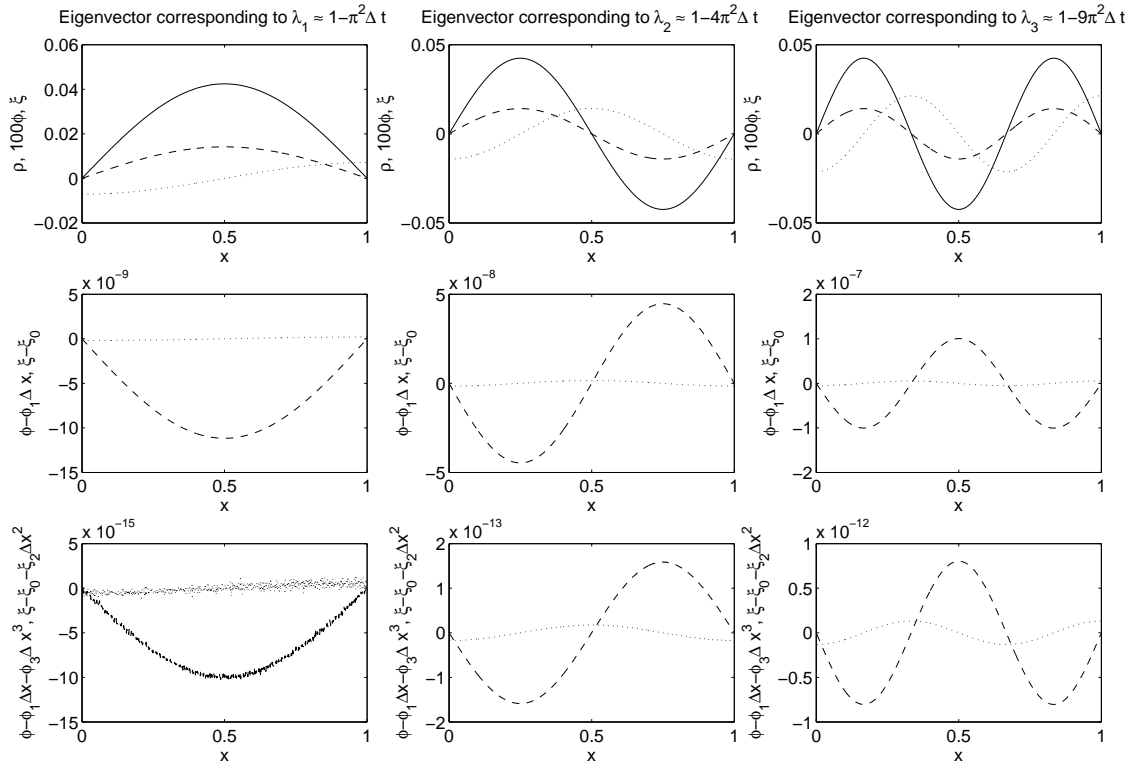


Figure 1: The eigenmodes corresponding to the three most dominant eigenvalues (first row) and a confirmation of the LBM slaving relations (second and third row). The solid, dotted and dashed line correspond to the density ρ , momentum ϕ and energy ξ components, respectively.

the derivatives were approximated with sufficiently accurate finite differences. The correctness of the equations (7) and (8) is clearly confirmed.

2.3 A time-stepper for the macroscopic equation

The macroscopic equation (6) can be solved analytically using the method of separation of variables. We obtain

$$\rho(x, t) = \sum_{k=1}^{\infty} A_k \exp(-Dk^2\pi^2 t) \sin(k\pi x), \quad A_k = 2 \int_0^1 \rho(x, 0) \sin(k\pi x) dx. \quad (9)$$

The parameter k is called the wave number. Alternatively, one may approximate the solution numerically. We then (again) obtain a discrete time-stepper (but now for the density field only). When using the standard second-order accurate central finite difference (FD) formula in space (with grid spacing Δx) and the forward Euler scheme in time (with time step Δt), we obtain

$$\rho_j^{n+1} = \rho_j^n + D \frac{\Delta t}{\Delta x^2} (\rho_{j+1}^n - 2\rho_j^n + \rho_{j-1}^n), \quad (10)$$

with ρ_j^n the approximation of the exact solution at time t_n and grid point x_j in the interior of the domain. As equation (10) is linear in ρ , the whole system can be written in matrix form $\rho^{n+1} = A \cdot \rho^n$, with ρ^n a column vector consisting of the elements ρ_j^n ($j = 1, \dots, N-1$). The Dirichlet boundary conditions are then explicitly eliminated and A is a tridiagonal matrix.

The truncation error $T(x, t)$ of the FD scheme (10) is defined as its residual divided by the step size Δt , when the exact solution $\rho(x_j, t_n)$ is substituted into the scheme. In this manner, the

Table 2: The three most dominant eigenvalues $\lambda_{1,2,3}$ of the PDE solution, the FD scheme and the LBM.

	λ_1	λ_2	λ_3
PDE	0.9999980260811	0.9999921043477	0.9999822348699
FD	0.9999980260807	0.9999921043425	0.9999822348436
LBM	0.9999980260805	0.9999921043383	0.9999822348225

truncation error scales like the global error; when $T(x, t) = \mathcal{O}(\Delta x^r + \Delta t^s)$, the method is said to be of order r in space and s in time. For the FD scheme (10), a Taylor series expansion can be used to show that the principal part of $T(x, t)$ is

$$\bar{T}(x, t) = \frac{\partial \rho}{\partial t} - D \frac{\partial^2 \rho}{\partial x^2} + \frac{1}{2} \frac{\partial^2 \rho}{\partial t^2} \Delta t - \frac{1}{12} D \frac{\partial^4 \rho}{\partial x^4} \Delta x^2 = \frac{1}{2} \frac{\partial^2 \rho}{\partial t^2} \Delta t - \frac{1}{12} D \frac{\partial^4 \rho}{\partial x^4} \Delta x^2. \quad (11)$$

Similar to the Fourier series of the analytical solution (9) of the macroscopic equation (6), we can write the numerical solution of the FD scheme as a discrete Fourier series of the form

$$\rho_j^n = \sum_{k=1}^{N-1} A_k (\lambda_k)^n \sin(k\pi x_j), \quad \lambda_k = 1 - 2D \frac{\Delta t}{\Delta x^2} (1 - \cos(k\pi \Delta x)).$$

The discrete Fourier modes $\sin(k\pi x_j)$ are now grid functions defined on the grid $\{x_j\}_{j=1}^{N-1}$ and correspond to the eigenvectors of the matrix A . The FD scheme is stable if all eigenvalues λ_k lie within the unit circle. Hence, the scheme is stable if $\Delta t \in (0, \Delta x^2/(2D))$. For values of Δt outside this interval, N can always be chosen such that the modes corresponding to the highest wave numbers grow unboundedly. At low wave numbers, the eigenvalues approximate the analytical eigenvalues

$$\exp(-Dk^2\pi^2\Delta t) - \lambda_k = \left(\frac{1}{2}\Delta t^2 - \frac{1}{12}D\Delta t\Delta x^2 \right) \pi^4 k^4 + \mathcal{O}(k^6), \quad k \rightarrow 0.$$

This clearly provides an alternative means to investigate the accuracy of the FD scheme, cf. (11).

As an illustration, the three most dominant eigenvalues of the PDE solution (9), of the FD scheme (10) and of the LBM from Section 2.1 are given in Table 2. Here, we used the same parameters that were also used to generate Figure 1. Clearly, the dominant eigenvalues of the three models correspond very well, indicating that (at least the long-term) behavior will be very similar. Of course, this is not the case for the less dominant eigenvalues, since those depend largely on the numerical discretization and are therefore not necessarily a good approximation of the eigenvalues of the exact solution. Note for instance that the eigenvalues of the PDE solution and the FD scheme are all real, while many of the eigenvalues of the LBM are complex. (An illustration of a typical eigenvalue spectrum of a LBM for a reaction-diffusion system can be found in [14, 19].)

In the remainder of this paper, we will perform a similar accuracy and stability analysis of the CTS for the LBM. As the primary goal of the CTS is to be an approximate time-stepper for the — in practice unknown — macroscopic equation, we expect to observe numerical properties that are similar to those of the FD scheme.

3 The CTS for the LBM

In this section, we show how to construct (several variants of) the CTS for the LBM. Without loss of generality, we set $D = 1$ from now on, which corresponds to rescaling time.

In general, we first have to choose an appropriate set of (possibly spatially distributed) macroscopic variables, for which we believe that a macroscopic description exists. Essential is that the

slow manifold referred to in Section 2.2 should be parameterizable in terms of these variables. For complex systems, choosing such macroscopic variables may be nontrivial. For the LBM from Section 2.1 however, we know that the effective macroscopic behavior is described by the PDE (9) for the density field $\rho(x, t)$, and that the slow manifold can be parameterized in terms of this variable, see (7)–(8). Therefore, the CTS for the LBM will be a time-stepper for only the density field (as the FD scheme in Section 2.3).

One coarse time step consists of (1) lifting, (2) simulation with the LBM and (3) restriction. In the following sections, we will formulate these three substeps in the specific context of our LBM. As each of these operations is linear, we are able to represent them using a constant Jacobian matrix. The CTS itself is then also a linear operation, and its Jacobian matrix is obtained by multiplying the Jacobian matrices of the individual substeps. In Section 4, this Jacobian matrix will be the starting point for the analysis of the accuracy and stability of the CTS.

3.1 Lifting

The main challenge in constructing the CTS for the LBM is to find an appropriate lifting procedure. For our model problem, the momentum ϕ and the energy ξ should be initialized according to the given density ρ . Ideally, they should correspond to the point in the LBM state space that corresponds to the given density ρ and lies on (or very close to) the slow manifold. This suggests that we can use the slaving relations (7)–(8) to implement the lifting procedure. However, such a procedure is mainly of theoretical interest, as in practice the (higher order) slaving relations are unlikely to be known and difficult to derive (otherwise, we may probably as well derive a macroscopic equation like (6)). We therefore also study an alternative lifting procedure, the so-called constrained runs scheme, which approximates the slaving relations numerically.

3.1.1 Lifting with the slaving relations

By using the slaving relations (7)–(8) up to (and, as always in this paper, including) $\mathcal{O}(\Delta x^p)$, and approximating the derivatives numerically, we obtain what will further be called the SR(p)-lifting scheme.

The corresponding Jacobian matrix $L_{\text{sr},p}$ is a rectangular matrix of size $(3N + 3) \times (N + 1)$, reflecting the one-to-many nature of the operation. As the density is given, the square upper submatrix is the identity matrix. The matrix elements for the two square lower submatrices correspond to an appropriate discretization of the truncated slaving relations. The important thing here is that the error introduced by the numerical approximation of the derivatives should be at least of order $\mathcal{O}(\Delta x^{p+1})$. In our experiments, we have chosen to approximate these derivatives using symmetric and antisymmetric central differences in the interior of the domain (near the boundaries, the use of one-sided differences is inevitable). Specifically, we approximated the first spatial derivative using the second-order accurate antisymmetric central difference stencil of size $2\Delta x$ when $p = 1$ or $p = 2$, or using the fourth-order accurate antisymmetric central difference stencil of size $4\Delta x$ when $p = 3$. The second spatial derivative was approximated using the second-order accurate symmetric central difference stencil of size $2\Delta x$ when $p = 2$ or $p = 3$. Finally, the third spatial derivative was approximated using the second-order accurate antisymmetric central difference stencil of size $4\Delta x$ when $p = 3$. These discretizations give rise to the Jacobian matrix elements shown in Table 3. Because we used symmetric and antisymmetric central differences, the square submatrices corresponding to the energy ξ and the momentum ϕ are symmetric and skew-symmetric, respectively, if we disregard some of the matrix elements near the boundaries.

3.1.2 Lifting with the constrained runs scheme

If the slaving relations are not known, the procedure from Section 3.1.1 cannot be used. As an alternative, one can then use the so-called constrained runs (CR) scheme [3]. This scheme relies on the fact that, under certain conditions, the computed microscopic state will lie close to the slow manifold if the $(m + 1)$ st time derivatives of the higher order moments are zero. Although it was

Table 3: The elements near the diagonal of the two square lower submatrices of the Jacobian matrix $L_{sr,p}$, corresponding to the numerical discretization of the slaving relations (7)–(8) up to order p .

	ϕ_0	$\phi_1\Delta x$	$\phi_1\Delta x + \phi_3\Delta x^3$	ξ_0	$\xi_0 + \xi_2\Delta x^2$
e_{-2}	0	0	$-(\omega^2 - \omega + 1)/(9\omega^3)$	0	0
e_{-1}	0	$1/(3\omega)$	$(5\omega^2 - 2\omega + 2)/(9\omega^3)$	0	$(2 - \omega)/(18\omega^2)$
e_0	0	0	0	$1/3$	$(1 + \omega)(3\omega - 2)/(9\omega^2)$
e_1	0	$-1/(3\omega)$	$-(5\omega^2 - 2\omega + 2)/(9\omega^3)$	0	$(2 - \omega)/(18\omega^2)$
e_2	0	0	$(\omega^2 - \omega + 1)/(9\omega^3)$	0	0

shown that using a larger value of m may result in a state that lies closer to the slow manifold [3], using a small value of m (e.g., $m = 0$) may already be sufficient for practical purposes. By approximating the $(m + 1)$ st time derivatives numerically using forward differences, the procedure can also be applied when only a time-stepper is available (as in our case). Under certain conditions, the zero of this $(m + 1)$ st forward difference equation may be computed using a functional iteration. The resulting scheme will further be called the CR(m)-lifting scheme. Specifically for our LBM, it takes the following form:

0. Initialize ϕ and ξ (e.g., $\phi = 0$ and $\xi = \rho/3$, corresponding to the BGK equilibrium distributions f_i^{eq} (2)). Then start the iteration 1–3.
1. Run the LBM over $m + 1$ time steps, starting from ρ, ϕ and ξ . This gives the values ρ_k, ϕ_k and ξ_k at times $t = k\Delta t$ ($k = 1, \dots, m + 1$).
2. Compute the forward differences $\delta_\phi = (-1)^m \Delta^{m+1} \phi$ and $\delta_\xi = (-1)^m \Delta^{m+1} \xi$ from ϕ_k and ξ_k ($k = 1, \dots, m + 1$).
3. If $\|\delta_\phi\|$ and $\|\delta_\xi\|$ are smaller than a certain tolerance: end the iteration.
Else: set $\phi = \phi + \delta_\phi$, $\xi = \xi + \delta_\xi$ and goto 1.

A close inspection of this scheme shows that, in each iteration step, the values of the higher order moments ϕ and ξ are updated using a backward extrapolation with a polynomial of degree m that passes through ϕ_k and ξ_k ($k = 1, \dots, m + 1$), while the density is reset to its original, given value.

In step 0 of the CR scheme, the $(N + 1)$ -dimensional density vector ρ is expanded to a $(3N + 3)$ -dimensional LBM state. Each iteration step of the scheme that is performed afterwards is linear and therefore corresponds to a multiplication with a constant Jacobian matrix $L_{cr,m}$. When $m = 0$, this Jacobian matrix corresponds to the matrix S from (5) in which $S_{1,1}$ is replaced by the identity matrix and $S_{1,2}$ and $S_{1,3}$ are replaced by zero matrices. From $L_{cr,0}$, we can derive to what values the initial values ϕ_j and ξ_j (the momentum and energy at grid position x_j) have evolved after K iteration steps of the CR(0)-lifting scheme. For values at the interior of the domain, we obtain

$$\phi_j^K = \sum_{l=1}^K \frac{\omega}{3} (1 - \omega)^{l-1} (\rho_{j-l} - \rho_{j+l}) + \frac{(1 - \omega)^K}{2} (\phi_{j-K} + \phi_{j+K}) + (1 - \omega)^K (\xi_{j-K} - \xi_{j+K}),$$

$$\xi_j^K = \sum_{l=1}^K \frac{\omega}{6} (1 - \omega)^{l-1} (\rho_{j-l} + \rho_{j+l}) + \frac{(1 - \omega)^K}{4} (\phi_{j-K} - \phi_{j+K}) + \frac{(1 - \omega)^K}{2} (\xi_{j-K} + \xi_{j+K}).$$

Expanding both equations using a Taylor series about $\Delta x = 0$ yields

$$\phi^K = (1 - \omega)^K \phi - 2 \frac{\frac{\partial \rho}{\partial x} - (1 - \omega)^K \left((K\omega + 1) \frac{\partial \rho}{\partial x} - 3K\omega \frac{\partial \xi}{\partial x} \right)}{3\omega} \Delta x + \frac{K^2 (1 - \omega)^K}{2} \frac{\partial^2 \rho}{\partial x^2} \Delta x^2 + \mathcal{O}(\Delta x^3),$$

$$\xi^K = \frac{\rho}{3} + (1-\omega)^K \left(\xi - \frac{\rho}{3} \right) - K \frac{(1-\omega)^K}{2} \frac{\partial \phi}{\partial x} \Delta x + \mathcal{O}(\Delta x^2).$$

When $K \rightarrow \infty$, we obtain

$$\begin{aligned} \phi^\infty &= -\frac{2}{3\omega} \frac{\partial \rho}{\partial x} \Delta x - \frac{1}{9\omega^3} (\omega^2 - 6\omega + 6) \frac{\partial^3 \rho}{\partial x^3} \Delta x^3 + \mathcal{O}(\Delta x^5), \\ \xi^\infty &= \frac{\rho}{3} - \frac{\omega - 2}{6\omega^2} \frac{\partial^2 \rho}{\partial x^2} \Delta x^2 + \mathcal{O}(\Delta x^4). \end{aligned}$$

From the derivation above it follows that the CR(0)-lifting scheme is stable for all values of $\omega \in (0, 2)$, and that it converges with an asymptotic convergence rate $|1 - \omega|$ towards a state that corresponds up to $\mathcal{O}(\Delta x)$ to the slaving relations (7)–(8). The same conclusions were found in [15], where a more detailed analysis was given for a class of LBMs for reaction-diffusion systems. From the slaving relations (7)–(8) and the formulas above, it follows that for our model problem, the constrained runs errors e_ϕ and e_ξ in the momentum and energy (the difference between ϕ^∞/ξ^∞ and the exact slaved momentum/energy) is

$$e_\phi \approx \frac{-2\omega^2 + 8\omega - 8}{9\omega^3} \frac{\partial^3 \rho}{\partial x^3} \Delta x^3, \quad e_\xi \approx \frac{2 - \omega}{9\omega^2} \frac{\partial^2 \rho}{\partial x^2} \Delta x^2.$$

A similar (but more technical) analysis can be done when $m > 0$. In this manner, one can for instance show that the CR(1)-lifting scheme converges towards a state that corresponds up to $\mathcal{O}(\Delta x^3)$ to the slaving relations (7)–(8), if the iteration is stable. Specifically, one can show that the constrained runs error e_ϕ in the momentum is now

$$\begin{aligned} e_\phi &\approx \frac{-13\omega^4 - 30\omega^3 + 350\omega^2 - 720\omega + 440}{540\omega^5} \frac{\partial^5 \rho}{\partial x^5} \Delta x^5 - \frac{-13\omega^4 + 50\omega^3 - 90\omega^2 + 80\omega - 40}{540\omega^5} \frac{\partial^5 \rho}{\partial x^5} \Delta x^5 \\ &= \frac{-4\omega^3 + 22\omega^2 - 40\omega + 24}{27\omega^5} \frac{\partial^5 \rho}{\partial x^5} \Delta x^5, \end{aligned}$$

while the constrained runs error e_ξ in the energy is

$$e_\xi \approx \frac{3\omega^3 - 26\omega^2 + 68\omega - 56}{216\omega^4} \frac{\partial^4 \rho}{\partial x^4} \Delta x^4 - \frac{\omega^3 - 6\omega^2 + 12\omega - 8}{72\omega^4} \frac{\partial^4 \rho}{\partial x^4} \Delta x^4 = \frac{-\omega^2 + 4\omega - 4}{27\omega^4} \frac{\partial^4 \rho}{\partial x^4} \Delta x^4.$$

Unfortunately, stability is no longer guaranteed for all values of ω when $m > 0$. The CR(1)-scheme for example is only stable if $\omega \in (0.690, 1.291)$ [16]. For values of ω outside this interval, the fixed point of the CR scheme can however still be computed, for instance using a Newton-Krylov technique [16].

3.2 Simulation

Starting from the initial condition provided by the lifting procedure, the LBM is evolved over a time interval ΔT . For simplicity, we assume that ΔT is a multiple of Δt . A simulation over time $\Delta T = M\Delta t$ then corresponds to a multiplication with the matrix S^M .

For complex (possibly stochastic or chaotic) microscopic systems, the choice of ΔT may be nontrivial (see e.g. [10]). Even for the deterministic LBM from Section 2.1, several scenarios are possible. From our discussion in Section 2.2, we know that if the initial condition lies on (or very close to) the slow manifold, no fast microscopic modes will be triggered in the first few LBM steps. Hence, ΔT may be chosen very small (e.g., $M \approx 1$). If the initial condition lies further away from the slow manifold, we should at least evolve until the fast modes have died out and the LBM state is again close enough to the slow manifold. Due to the separation of time scales, the time required to approach the manifold will only be a small multiple of the LBM time step Δt (e.g., $M \approx 10$). Nevertheless, obtaining a slaved state at time ΔT is not always sufficient, as the trajectory that is followed on the slow manifold afterwards may still be different from the correct macroscopic trajectory that would be obtained if we had initialized directly on the slow manifold

[14, 19]. In certain situations, the effect of the inaccurate initialization becomes less prominent if ΔT is chosen very large (e.g., $M > 1000$), for instance in the case where all trajectories are ultimately attracted towards the same steady state [14] — we will come back to this in Section 4.2.1. However, using such a large time step ΔT will often be unacceptable in practice, especially when using the corresponding CTS in conjunction with efficiency-increasing algorithms such as coarse projective integration or when using the CTS as a building block in a time-stepper based bifurcation analysis (the attainable efficiency gain then drops substantially, and computing (near) unstable solutions may become impossible).

3.3 Restriction

Finally, in the restriction step, we should go back from the space of LBM variables (as we are using the moment description, these are ρ , ϕ and ξ) to the space of macroscopic variables (here, ρ). This is a trivial operation and the corresponding Jacobian matrix R is a $(N + 1) \times (3N + 3)$ matrix (reflecting its many-to-one nature), with the square left submatrix the identity matrix and the square right submatrices zero matrices.

4 Accuracy and stability of the CTS

In this section, we are finally ready to study the accuracy and stability of the CTS. The main idea is that we will explicitly construct the Jacobian matrices of several variants of the CTS, using the components described in the previous section. Similar to the analysis of the FD scheme in Section 2.3, we will then use the Jacobian matrix elements to derive the truncation error and the stability interval for the different variants of the CTS. In Section 4.1, we consider the CTS in the special case where $M = 1$ ($\Delta T = \Delta t$). The influence of using a larger value of M is explored in Section 4.2.

4.1 The CTS with $M = 1$

We make a further distinction between the CTS that uses SR(p)-lifting and the CTS that is based on CR(m)-lifting.

4.1.1 Using SR(p)-lifting

In this case, the Jacobian matrix of the CTS is $RSL_{sr,p}$. For each value of p , its elements can be computed using the results from Section 3. A summary is given in Table 4. Since we opted to use only (anti-)symmetric central differences, the Jacobian matrix is now symmetric if we disregard some of the matrix elements near the boundaries. Slightly remarkable (at least at first sight) is the fact that when $\omega = 1$, the CTS corresponds to the FD scheme (10) irrespective of the value of p , while the SR(p)-lifting schemes are different for each value of p (cf. Table 3). The reason is of course that after the diffusive collisions, the three distribution functions in the LBM coincide ($f_i = f_i^{eq} = \rho/3$), and then there is no difference in using the LBM or the FD scheme.

We now use the matrix elements from Table 4 to compute the principal part of the truncation error for the different CTSs (compared to the macroscopic solution (9)). The results are shown in Table 5. We see that when $p = 0$ (this corresponds to initializing with the BGK equilibrium distributions (2)), the CTS does not recover the correct macroscopic behavior unless in the special case $\omega = 1$. When $p = 0$ and $\omega \neq 1$, the solution computed with the CTS can be interpreted as an approximation to the solution of the diffusion equation with a modified diffusion coefficient $D' = \Delta x^2 / (3\Delta t) = \omega / (2 - \omega)$ instead of $D = 1$.

When $p = 1, 2$ or 3 and assuming that $\Delta t = \mathcal{O}(\Delta x^2)$ (which is the most natural choice for a diffusion LBM, but was not assumed in the derivation of the expressions in Table 5), the CTS is first-order accurate in time and second-order accurate in space for all values of ω . If Δt decreases faster than $\mathcal{O}(\Delta x^4)$, the truncation error grows unboundedly in the cases $p = 1$ or $p = 2$ and the CTS is then no longer consistent. Similarly, the truncation error grows unboundedly if Δt

Table 4: The elements near the diagonal of the Jacobian matrix of the CTS, when $M = 1$ ($\Delta T = \Delta t$) and using SR(p)-lifting.

	$p = 0$	$p = 1$	$p = 2$	$p = 3$
e_0	1/3	$(2\omega - 1)/(3\omega)$	$(3\omega^2 - 4\omega + 2)/(3\omega^2)$	$(11\omega^3 - 16\omega^2 + 10\omega - 2)/(9\omega^3)$
$e_{\pm 1}$	1/3	1/3	$(\omega^2 + 6\omega - 4)/(9\omega^2)$	$(\omega^3 + 14\omega^2 - 10\omega + 1)/(18\omega^3)$
$e_{\pm 2}$	0	$(1 - \omega)/(6\omega)$	$(1 - \omega^2)/(9\omega^2)$	$(1 - \omega)(2\omega^2 + 1)/(9\omega^3)$
$e_{\pm 3}$	0	0	0	$(1 - \omega)(-\omega^2 + \omega - 1)/(18\omega^3)$

Table 5: The principal part of the truncation error $\bar{T}(x, t)$ and the stability interval $(\omega_{\min}, \omega_{\max})$ for the CTS, when $M = 1$ ($\Delta T = \Delta t$) and using SR(p)-lifting.

	Principal part of the truncation error $\bar{T}(x, t)$	Stability interval
$p = 0$	$\frac{\partial \rho}{\partial t} - \frac{\Delta x^2}{3\Delta t} \frac{\partial^2 \rho}{\partial x^2}$	$(0, 2)$
$p = 1$	$\frac{1}{2} \frac{\partial^2 \rho}{\partial t^2} \Delta t - \frac{1}{3} \frac{\partial^4 \rho}{\partial x^4} \Delta x^2 + \frac{1}{12} \frac{\partial^4 \rho}{\partial x^4} \frac{\Delta x^4}{\Delta t}$	$(\frac{8}{13} - \frac{2}{13}\sqrt{3}, 2) \approx (0.349, 2)$
$p = 2$	$(\frac{1}{2} \frac{\partial^2 \rho}{\partial t^2} - \frac{1}{4} \frac{\partial^4 \rho}{\partial x^4}) \Delta t - \frac{1}{4} \frac{\partial^4 \rho}{\partial x^4} \Delta x^2 + \frac{1}{12} \frac{\partial^4 \rho}{\partial x^4} \frac{\Delta x^4}{\Delta t}$	$(-3 + \sqrt{13}, 2) \approx (0.606, 2)$
$p = 3$	$\frac{3}{4} \frac{\partial^4 \rho}{\partial x^4} \frac{\Delta t^2}{\Delta x^2} + \mathcal{O}(\Delta t^2, \Delta x^4, \Delta x^2 \Delta t, \Delta x^6 / \Delta t)$	$(-3 + \sqrt{13}, 2) \approx (0.606, 2)$

decreases slower than $\mathcal{O}(\Delta x)$ or faster than $\mathcal{O}(\Delta x^6)$ when $p = 3$. If the value of Δx is kept constant, the CTS with $p = 3$ behaves second-order accurate in time when $\Delta t > \mathcal{O}(\Delta x^{8/3})$ (while the error increases as $1/\Delta t$ when $\Delta t < \mathcal{O}(\Delta x^{8/3})$). Note that the LBM itself is also second-order accurate in time when using a fixed lattice spacing, and first-order accurate in time and second-order accurate in space when ω is kept constant [7, 19]. This indicates that for $\Delta t > \mathcal{O}(\Delta x^{8/3})$, the SR(3)-lifting scheme is so accurate that the error of the CTS has reached the error level of the LBM itself (compared to the macroscopic equation (6)). In Section 4.1.2, this claim will be confirmed.

Similar to the Fourier series of the analytical solution of the PDE (6) itself, we can decompose the numerical solution of the CTS in terms of the orthogonal eigenvectors of the corresponding Jacobian matrix. As one-sided finite differences are used near the boundaries of the spatial domain, it is no longer guaranteed that, after elimination of the boundary conditions, these eigenmodes are $\sin(k\pi x_j)$, $k = 1, \dots, N - 1$. A common practice in numerical analysis is therefore to resort to a local Fourier analysis, which ignores the effects of the boundaries. Then, $\sin(k\pi x_j)$ are still the eigenmodes and the corresponding eigenvalues λ_k are given by the formula

$$\lambda_k = \sum_{i=-\infty}^{i=+\infty} e_i \cos(k\pi i \Delta x) = e_0 + \sum_{i=1}^{\infty} 2e_i \cos(k\pi i \Delta x), \quad (12)$$

where e_i are the elements from Table 4. At low wave numbers, the eigenvalues approximate the analytical eigenvalues from equation (9), and the principal part of the Taylor series expansion of $\exp(-k^2 \pi^2 \Delta t) - \lambda_k$ (for $k \rightarrow 0$) corresponds to $\bar{T}(x, t) \Delta t$ if we substitute $\partial^{2i} \rho / \partial x^{2i}$ and $\partial \rho^i / \partial t^i$ by $k^{2i} \pi^{2i}$ in the latter. The CTS is stable if all eigenvalues λ_k lie within the unit circle. Using

equation (12), we can hence derive the stability intervals for the different CTSs (i.e., the intervals of ω for which the CTSs are stable). The results are shown in Table 5. If $p = 0$, the eigenvalues lie between $-1/3$ and 1 and the CTS is unconditionally stable (i.e., it is stable for all values of $\omega \in (0, 2)$). If $p = 1$, the eigenmodes corresponding to the intermediate wave numbers become unstable when $\omega < 0.349$. If $p = 2$, the eigenmodes corresponding to the highest wave numbers become unstable when $\omega < 0.606$. Finally, if $p = 3$, the eigenmodes corresponding to both the intermediate and the highest wave numbers become unstable when $\omega < 0.606$.

4.1.2 Using CR(m)-lifting

When we use K CR iteration steps and the BGK equilibrium distributions (2) as initial guess, the Jacobian matrix of the CTS is $RSL_{\text{cr},m}^K L_{\text{st},0}$. For simplicity, we first consider the case $m = 0$. The number of nonzero elements in each row and column of the Jacobian matrix (far enough away from the boundaries) is then $2K + 3$. If $K = 0$, we obtain the SR(0)-lifting scheme from the previous section. If $K \geq 1$, the elements of the symmetric Jacobian matrix are

$$\begin{aligned} e_0 &= 1 - \frac{2}{3}\omega, & e_{\pm i} &= \frac{1}{3}\omega^2(1-\omega)^{i-1} \quad (i = 1, \dots, K-1), \\ e_{\pm K} &= \frac{1}{3}(2\omega-1)(1-\omega)^{K-1}, & e_{\pm(K+1)} &= \frac{1}{3}(1-\omega)^K. \end{aligned} \quad (13)$$

Using these elements, one can derive the truncation error of the corresponding CTS. After some calculations, we obtain

$$\bar{T}(x, t) = \frac{\partial \rho}{\partial t} - \left(\frac{\omega - 2 + 2(1-\omega)^{K+1}}{\omega - 2} \right) \frac{\partial^2 \rho}{\partial x^2}. \quad (14)$$

For small values of K , the CTS does not recover the correct macroscopic behavior, unless $\omega = 1$. If $\omega = 1$, the CTS corresponds to the CTS based on the SR(0)-lifting scheme without additional CR steps, and hence also to the FD scheme (10). If $\omega \neq 1$, the solution computed with the CTS can again be interpreted as an approximation to the solution of the diffusion equation with a modified diffusion coefficient D' (the factor between large brackets in (14)) instead of $D = 1$. It is clear that D' differs more from the correct value $D = 1$ as ω deviates more from one. As K grows, D' converges fast to one (linearly, and with the same convergence rate $|1 - \omega|$ as the CR(0)-lifting scheme itself). The fact that the CTS reproduces the correct macroscopic behavior if $K \rightarrow \infty$ should not surprise us, as we have shown in Section 3.1.2 that the order of accuracy of the CR(0)-lifting scheme is the same as the order of accuracy of the SR(1)-lifting scheme, and we have shown in Section 4.1.1 that the CTS based on the SR(1)-lifting scheme reproduces the correct macroscopic behavior. Of course, the truncation error is different. If $K \rightarrow \infty$, the right-hand side of equation (14) becomes zero and the principal part of the truncation error is then

$$\bar{T}(x, t) = \frac{1}{2} \frac{\partial^2 \rho}{\partial t^2} \Delta t + \left(\frac{1}{6} \Delta x^2 - \frac{27}{12} \frac{\Delta t^2}{\Delta x^2} \right) \frac{\partial^4 \rho}{\partial x^4}.$$

If $\Delta t = \mathcal{O}(\Delta x^2)$, the CTS is again first-order accurate in time and second-order accurate in space for all values of ω . If Δt decreases slower than $\mathcal{O}(\Delta x)$, the truncation error grows unboundedly and the CTS is no longer consistent.

After elimination of the boundary conditions, the eigenvectors of the Jacobian matrix of the CTS are the discrete Fourier modes $\sin(k\pi x_j)$. Hence, the corresponding eigenvalues λ_k are given by (12), now with e_i the elements from (13). As before, the eigenvalues at low wave numbers approximate the analytical eigenvalues from equation (9), and the difference between both is related to the accuracy. From the eigenvalues we compute the stability intervals of the CTS for different values of K . An overview is given in Table 6. The stability intervals clearly evolve from $(1/2, 5/4)$ if $K = 1$ towards the limiting interval $(0, 6/5)$ if $K \rightarrow \infty$. So, although the constrained runs scheme is stable and finds a LBM state close to the slow manifold as $K \rightarrow \infty$, the CTS itself

Table 6: The boundaries of the stability interval $(\omega_{\min}, \omega_{\max})$ of the CTS, when $M = 1$ ($\Delta T = \Delta t$) and using a lifting that consists of K CR(0) iteration steps, starting from the BGK equilibrium distributions.

	$K=0$	$K=1$	$K=2$	$K=3$	$K=4$	$K=6$	$K=8$	$K=25$	$K=100$	$K=\infty$
ω_{\min}	0.000	0.500	0.388	0.352	0.305	0.253	0.217	0.107	0.038	0.000
ω_{\max}	2.000	1.250	1.207	1.201	1.200	1.200	1.200	1.200	1.200	1.200

is unstable for a large range of ω -values. Remarkable is also that the CTS becomes unstable if Δt becomes too *small* compared to Δx^2 .

If $m > 0$, the accuracy and stability can be analyzed in a similar manner. Due to page limitations, we here only mention that numerical experiments indicate that when $\Delta t = \mathcal{O}(\Delta x^2)$, the principal part of the truncation error of the CTS based on the infinitely iterated CR(1)-lifting scheme is the same as that of the CTS based on SR(3)-lifting. This confirms our finding in the last paragraph of Section 3.1.2. Moreover, it indicates that both lifting schemes are so accurate that the error of the CTS is now dominated by the error of the LBM itself (the difference between the LBM and the macroscopic equation (6)), rather than only being at the same level as the error of the LBM as was stated in Section 4.1.1. This is also confirmed by numerical experiments that show that the error of the CTS is virtually the same as the error of a full LBM, when the latter is only initialized once at the beginning of the simulation interval. We emphasize that this is the best one can hope for; the fact that the expressions for the truncation error in Table 5 do not further tend towards zero is because we are comparing to the macroscopic solution rather than to the full LBM solution. If we compare to the solution of the full LBM (by also incorporating higher order terms in the Chapman-Enskog multiscale expansion), we find that the truncation errors are the expressions from Table 5 minus $(3\Delta t^2/(4\Delta x^2))\partial^4\rho/\partial x^4$. This shows that the truncation error does decrease as p increases, and that for $p = 3$ the truncation error is indeed dominated by the error of the LBM. Of course, the stability of the CTS based on the infinitely iterated CR(1)-lifting and the CTS based on SR(3)-lifting is different. While the stability interval was $(0.606, 2)$ in the case of SR(3)-lifting, it is only $(0.690, 1.101)$ in the case of CR(1)-lifting. Note that the latter is in line with the stability of the CR(1)-lifting scheme itself, cf. Section 3.1.2.

4.2 The CTS with $M > 1$

In the previous section we showed that, depending on the lifting procedure, the accuracy and/or the stability of the CTS may be unsatisfactory if only one LBM time step is used in the simulation step, i.e., if $M = 1$ ($\Delta T = \Delta t$). In this section, we argue that both shortcomings may — at least partially — be resolved by using a larger value of M .

4.2.1 Improving the accuracy of the CTS

Let us reconsider the CTS that is based on SR(0)-lifting. When using M LBM simulation steps, the Jacobian matrix of the CTS is $RS^ML_{\text{sr},0}$. The number of nonzero elements in each row and column of the Jacobian matrix (far enough away from the boundaries) is then $2M+1$. The analysis for the case $M = 1$ was given in Section 4.1.1. If $M > 1$, the elements of the Jacobian matrix can again be computed explicitly. Although these elements themselves are rather complicated (and therefore omitted here), the principal part of the truncation error simplifies to

$$\bar{T}(x, t) = \frac{\partial \rho}{\partial t} - \left(1 + \frac{2}{M} \frac{\omega - 1}{\omega(\omega - 2)} (-1 + (1 - \omega)^M) \right) \frac{\partial^2 \rho}{\partial x^2}. \quad (15)$$

Note that the truncation error is now the residual divided by $\Delta T = M\Delta t$ when the exact solution is substituted into the scheme. As could be expected, the CTS does not recover the correct macroscopic behavior for finite values of M , unless $\omega = 1$. If $\omega \neq 1$, the solution computed with the CTS can again be interpreted as an approximation to the solution of the diffusion equation

Table 7: First row: the lower bound of the stability interval ($\omega_{\min}, 2$) as a function of M , when the CTS is based on the SR(1)-lifting scheme. Second row: the upper bound of the stability interval ($0, \omega_{\max}$) as a function of M , when the CTS is based on the infinitely iterated CR(0)-lifting scheme.

	$M=1$	$M=2$	$M=3$	$M=4$	$M=5$	$M=6$	$M=7$	$M=8$	$M=9$	$M=10$
ω_{\min}	0.349	0.310	0.311	0.268	0.231	0.227	0.213	0.198	0.184	0.177
ω_{\max}	1.200	1.500	1.500	1.500	1.858	1.583	1.653	1.708	1.655	1.814

with a modified diffusion coefficient $D' = 1 + \Delta D$ (the factor between large brackets in (14)) instead of $D = 1$. It is clear that ΔD differs more from zero as ω deviates more from one. As M grows towards infinity, ΔD converges to zero. This basically tells us that the CTS becomes more accurate (or rather, less inaccurate) when M is increased. The underlying reason is that the “bad” SR(0)-lifting then occurs less frequently when integrating over a certain fixed time interval with the CTS. Unfortunately, equation (15) also shows that ΔD only converges slowly (sublinearly, $\sim 1/M$) towards zero — compare with the fast linear convergence in the case of using CR(0)-lifting (Section 4.1.2). Hence, unless ω lies extremely close to one, M will have to be chosen very large in order to obtain accurate results. To get the modified diffusion coefficient D' for instance within 0.1% of the correct value $D = 1$, it is required that $M > 533$ if $\omega = 1.25$, $M > 1333$ if $\omega = 1.5$ and $M > 3428$ if $\omega = 1.75$. As already mentioned in Section 3.2, using such large values of M will in practice often be unacceptable.

After elimination of the boundary conditions, the eigenvectors of the Jacobian matrix of the CTS are again the discrete Fourier modes $\sin(k\pi x_j)$, and the corresponding eigenvalues λ_k are given by (12). As before, the eigenvalues at low wave numbers approximate the analytical eigenvalues from equation (9), and the difference between both is related to the accuracy. If M is increased, the eigenvalues shift towards zero and, as could be expected, the CTS remains unconditionally stable. If we started a simulation from the (scaled) k -th Fourier mode as initial condition, the relative error made due to the fact that $\Delta D \neq 0$ would approximately be $1 - \exp(-(\Delta D)k^2\pi^2 t)$. Taking into account that $\Delta D = \mathcal{O}(1/M)$ as $M \rightarrow \infty$, and using $t = \Delta T = M\Delta t$, we thus obtain that the relative error made in each step of the CTS will approximately be independent of the value of M . This confirms that using larger values of M (and hence lifting less frequently) is indeed beneficial for the accuracy of the CTS.

4.2.2 Improving the stability of the CTS

Finally, we also consider the CTS based on SR(1)-lifting and on the infinitely iterated CR(0)-lifting (the initial guess is then irrelevant) when using M LBM simulation steps. After elimination of the boundary conditions, the eigenvectors of the Jacobian matrices are in both cases again the discrete Fourier modes $\sin(k\pi x_j)$, and the corresponding eigenvalues λ_k are given by (12). From these eigenvalues, we can deduce the different stability intervals. An overview is given in Table 7. We clearly recognize the limited stability intervals in the case $M = 1$ (cf. Sections 4.1.1 and 4.1.2), and observe that for both lifting schemes, the stability interval indeed grows (although not monotonically) when the value of M is increased.

5 Conclusions

The equation-free framework for multiscale computing is built around the central idea of a coarse time-stepper (CTS), which is an approximate time integrator for the unavailable macroscopic model when only a microscopic simulator is given. In this paper, we have studied the numerical properties of the CTS when a lattice Boltzmann model (LBM) for one-dimensional diffusion is used as the microscopic simulator.

For this model problem, we derived analytical expressions for the accuracy and stability of the

CTS. These expressions depend on the LBM parameters but also on the implementation of the CTS. It was shown that an accurate lifting procedure (using the theoretical slaving relations, or purely numerical, using the constrained runs scheme) is crucial to recover the correct macroscopic behavior. If the lifting is inaccurate, the CTS approximates a different macroscopic equation, and an erroneous macroscopic trajectory is computed. If the lifting is very accurate, its influence is negligible, and the accuracy of the CTS is similar to that of the underlying LBM itself. Concerning the stability of the CTS, we showed that in many cases there exist values of the LBM relaxation coefficient for which the CTS is unstable. Increasing the coarse time step ΔT may help to resolve both the accuracy and stability issues. However, increasing the time step too much is in practice often unacceptable, especially when using the CTS in conjunction with efficiency-increasing algorithms such as coarse projective integration or when using the CTS as a building block in a time-stepper based bifurcation analysis.

The analysis presented in this paper contributes substantially to the understanding of the numerical results in [13, 6, 8, 14, 15], in which various aspects of the equation-free approach were studied using a similar LBM as the microscopic simulator. Moreover, the results may also be useful for the further analysis and/or development of the equation-free methodology and its application to more complex microscopic models, for which the analysis may be much more complicated.

Acknowledgements

This paper presents research results of the Belgian Network DYSCO (Dynamical Systems, Control, and Optimization), funded by the Interuniversity Attraction Poles Programme, initiated by the Belgian State, Science Policy Office. The scientific responsibility rests with its author(s).

References

- [1] B. Chopard, A. Dupuis, A. Masselot, and P. Luthi. Cellular automata and lattice Boltzmann techniques: An approach to model and simulate complex systems. *Advances in Complex Systems*, 5(2/3):103–246, 2002.
- [2] W. E. Analysis of the heterogeneous multiscale method for ordinary differential equations. *Communications in Mathematical Sciences*, 1(3):423–436, 2003.
- [3] C. W. Gear, T. J. Kaper, I. G. Kevrekidis, and A. Zagaris. Projecting to a slow manifold: Singularly perturbed systems and legacy codes. *SIAM Journal on Applied Dynamical Systems*, 4(3):711–732, 2005.
- [4] C. W. Gear and I. G. Kevrekidis. Projective methods for stiff differential equations: Problems with gaps in their eigenvalue spectrum. *SIAM Journal of Scientific Computing*, 24(4):1091–1106, 2003.
- [5] C. W. Gear and I. G. Kevrekidis. Telescopic methods for parabolic differential equations. *Journal of Computational Physics*, 187(1):95–109, 2003.
- [6] C. W. Gear, I. G. Kevrekidis, and C. Theodoropoulos. Coarse integration/bifurcation analysis via microscopic simulators: Micro-Galerkin methods. *Computers and Chemical Engineering*, 26(7/8):941–963, 2002.
- [7] D. J. Holdych, D. R. Noble, J. G. Georgiadis, and R. O. Buckius. Truncation error analysis of lattice Boltzmann methods. *Journal of Computational Physics*, 193(2):595–619, 2004.
- [8] I. G. Kevrekidis, C. W. Gear, J. M. Hyman, P. G. Kevrekidis, O. Runborg, and C. Theodoropoulos. Equation-free, coarse-grained multiscale computation: Enabling microscopic simulators to perform system-level analysis. *Communications in Mathematical Sciences*, 1(4):715–762, 2003.
- [9] S. L. Lee and C. W. Gear. Second-order accurate projective integrators for multiscale problems. *Journal of Computational and Applied Mathematics*, 201(1):258–274, 2007.
- [10] A. G. Makeev, D. Maroudas, and I. G. Kevrekidis. Coarse stability and bifurcation analysis using stochastic simulators: Kinetic Monte Carlo examples. *Journal of Chemical Physics*, 116(23):10083–10091, 2002.

- [11] Y. H. Qian and S. A. Orszag. Scalings in diffusion-driven reaction $A + B \rightarrow C$: Numerical simulations by lattice BGK models. *Journal of Statistical Physics*, 81(1/2):237–253, 1995.
- [12] C. I. Siettos, M. D. Graham, and I. G. Kevrekidis. Coarse Brownian dynamics for nematic liquid crystals: Bifurcation, projective integration and control via stochastic simulation. *Journal of Chemical Physics*, 118(22):10149–10157, 2003.
- [13] C. Theodoropoulos, Y. H. Qian, and I. G. Kevrekidis. “Coarse” stability and bifurcation analysis using time-steppers: A reaction-diffusion example. *Proceedings of the National Academy of Sciences*, 97(18):9840–9843, 2000.
- [14] P. Van Leemput, K. Lust, and I. G. Kevrekidis. Coarse-grained numerical bifurcation analysis of lattice Boltzmann models. *Physica D: Nonlinear Phenomena*, 210(1–2):58–76, 2005.
- [15] P. Van Leemput, W. Vanroose, and D. Roose. Mesoscale analysis of the equation-free constrained runs initialization scheme. *Multiscale Modeling and Simulation*, 2007. Accepted.
- [16] C. Vandekerckhove, I. G. Kevrekidis, and D. Roose. An efficient Newton-Krylov implementation of the constrained runs scheme for initializing on a slow manifold. Technical Report TW 502, Katholieke Universiteit Leuven, Department of Computer Science, September 2007. Submitted.
- [17] C. Vandekerckhove and D. Roose. Accuracy analysis of acceleration schemes for stiff multiscale problems. *Journal of Computational and Applied Mathematics*, In press, 2007.
- [18] C. Vandekerckhove, D. Roose, and K. Lust. Numerical stability analysis of an acceleration scheme for step size constrained time integrators. *Journal of Computational and Applied Mathematics*, 200(2):761–777, 2007.
- [19] C. Vandekerckhove, P. Van Leemput, and D. Roose. Acceleration of lattice Boltzmann models through state extrapolation: A reaction-diffusion example. Technical Report TW 466, Katholieke Universiteit Leuven, Department of Computer Science, August 2006. Submitted.